Bacteria solve the problem of crowding by moving slowly

O. J. Meacock[1,2,3]†, A. Doostmohammadi[4]†, K. R. Foster[1,2]*, J. M. Yeomans[4]*, W. M. Durham[1,3]*

1. Department of Zoology, University of Oxford, Oxford, United Kingdom

2. Department of Biochemistry, University of Oxford, Oxford, UK

3. Department of Physics and Astronomy, University of Sheffield, Hounsfield Road, Sheffield, S3 7RH, United Kingdom

4. Rudolf Peierls Centre for Theoretical Physics, Clarendon Laboratory, Parks Road, University of Oxford, Oxford, OX1 3PU, United Kingdom

* e-mail: kevin.foster@zoo.ox.ac.uk, julia.yeomans@physics.ox.ac.uk, or w.m.durham@sheffield.ac.uk

†These authors contributed equally.

Bacteria commonly live attached to surfaces in very dense collectives containing billions of cells[1]. While it is known that motility allows these groups to expand en masse into new territory[2–5], how bacteria collectively move across surfaces under such tightly packed conditions remains poorly understood. Here we combine experiments, cell tracking and individual-based modelling to study the pathogen *Pseudomonas aeruginosa* as it collectively migrates across surfaces using grappling-hook like pili[3,6,7]. We show that the fast moving cells of a hyperpilated mutant are overtaken and outcompeted by the slower moving wild-type at high cell densities. Using theory developed to study liquid crystals[8–13], we demonstrate that this effect is mediated by the physics of topological defects, points where cells with different orientations meet one another. Our analyses reveal that when defects with topological charge +1/2 collide with one another, the fast-moving mutant cells rotate to point vertically and become trapped. By moving more slowly, wild-type cells avoid this trapping mechanism, allowing them to collectively migrate faster. Our work demonstrates that the physics of liquid crystals explains why slow bacteria can outcompete fast moving cells when competing for new territory.

Bacteria generate collective motility on surfaces through a variety of mechanisms[2–5,14]. While flagellar-based swimming in three dimensions is perhaps the best understood form of bacterial locomotion, swimming cells must be concentrated by orders of magnitude for collective behaviours to emerge, which are typically disrupted within minutes by oxygen depletion[15,16]. In contrast, groups of bacteria can spontaneously generate collective motility when pulling themselves across two-dimensional surfaces using twitching motility, which is instead driven by grappling hook-like appendages called Type-IV pili[3,6,7]. Here we study the relationship between individual and collective twitching motility within large groups of the opportunistic pathogen *P. aeruginosa*. We focus on movement in subsurface colonies sandwiched between agar and a coverslip (Fig. 1a), where movement is driven by pili, not flagella (Extended Data Fig. 1a,b), and where high-resolution time-lapse imaging can be used to follow individual cells as they collectively move along the glass surface. However, the phenomena we describe are not specific to this one assay. We also show that the key features are reproduced in classical bacterial colonies grown on the surface of agar (Fig. 1a-d, Extended Data Fig. 2, Supplementary Video 1).

Recent microfluidic experiments have shown that deleting the *pilH* gene, which encodes a response regulator in the two component system that regulates twitching motility[17], causes cells to move faster than wild-type (WT) cells[18], likely because they express a larger number of pili[17]. To confirm that this increase in speed also occurs in subsurface colonies, we developed a cell tracking algorithm to record the movement of thousands of individual cells within a single field of view (Methods, Supplementary Video 2). This revealed that individual Δ*pilH* cells move approximately twice as fast as WT cells in both densely packed collectives (Fig. 1e, Extended Data Fig. 3a) and at lower cell densities (Extended Data Fig. 3b). However, this difference in individual cell speed did not translate to how quickly colonies spread across the surface. While the faster motility of Δ*pilH* cells allowed them to initially spread outwards faster

2

than WT cells, their expansion rate plateaued after four hours. In contrast, the expansion rate of WT colonies steadily increased over a period of approximately six hours, eventually reaching a value four times greater than that of $\Delta pilH$ colonies and ten times greater than that of colonies of the non-piliated $\Delta pilB$ strain (Fig. 1f, g, Supplementary Video 3). An increase in individual motility, therefore, did not translate successfully to an increase in collective motility.

Previous work has shown that strains which dominate the nutrient-rich edge of colonies can obtain a substantial growth advantage[19]. To investigate how this might affect the competitive ability of $\Delta pilH$ cells, we inoculated surficial colonies with equal proportions of $\Delta pilH$ and WT cells. This revealed that $\Delta pilH$ cells remained trapped in the nutrient poor interior of the colony, while WT cells migrated outwards (Fig. 2a), allowing the latter to undergo approximately three more cell divisions over a 48-hour period (Fig. 2b). We next analysed the dynamics of this competition in greater detail using subsurface colonies and automated image analysis to simultaneously measure colony expansion rate, cell packing fraction, and genotypic composition (Fig. 2c-g, Supplementary Fig. 1, Supplementary Video 4, Supplementary Methods). Consistent with their initial rapid expansion in monoculture colonies, $\Delta pilH$ cells initially outnumbered WT cells at the expanding edge of the colony (hereafter "the front"). However, once the front transitioned from loosely packed groups of cells to a confluent monolayer (Fig. 2e, g), the colony expansion rate rapidly increased from 0.75 μm min^{-1} to 5.0 μm min^{-1} (Fig. 2d) while the proportion of $\Delta pilH$ cells at the front fell sharply, dropping from 82% at 200 min to 3% at 350 min (Fig. 2f).

What could be responsible for this rapid decline of $\Delta pilH$ despite its faster individual movement? Direct observation of the colony monolayer at the same time as the precipitous decline of fast moving $\Delta pilH$ cells suggested that $\Delta pilH$ cells lack the ability to move collectively and were more likely to become trapped in place than WT cells (Supplementary Video 5). To understand how the collective behaviours of the two strains differ, we turned to

tools originally developed to study liquid crystals. Densely packed cells tend to align in the same direction[2], and this nematic ordering produces collective movement on length scales substantially larger than that of a single cell[20,21]. Moreover, we observed that topological defects, an emergent feature of nematic systems, move about within the monolayer of cells (Supplementary Video 6, Methods). The two types of defects, with a topological change +1/2 and -1/2 respectively, Fig. 3a-c, denoted here as "comets" and "trefoils", are generated and annihilated in pairs (Extended Data Fig. 4a, b), as predicted by theory[8,9].

To investigate the physical properties of defects, we developed automated tools to combine single-cell tracking data collected across hundreds of defects. This revealed that the movements of both WT cells (Fig. 3d) and $\Delta pilH$ cells (Extended Data Fig. 4c) around comets and trefoils closely match predictions from both an individual-based model of self-propelled rods (SPR)[15] and a continuum model of active nematics[10], though $\Delta pilH$ flowfields are larger in scale than those of the WT. Theory predicts that comets migrate along their axis at a speed proportional to the activity of the nematic, a measure of the force exerted by each of the individuals that make up the system. In contrast, trefoils are predicted to move diffusively[11]. Consistent with this, we observed that the root mean squared displacement (RMSD) of comets was larger in $\Delta pilH$ monolayers than in WT monolayers, while the RMSD of trefoils was similar in both genotypes (Fig. 3e, f). These observations indicate that both WT and $\Delta pilH$ monolayers behave as an active nematic, with the latter possessing greater activity.

Comets elastically repel one another in a nematic confined to two dimensions[12]. However, previous theoretical predictions[9,13] and experiments with liquid crystals[13] suggested that when the nematic is allowed to reorient out of the 2D plane, two comets with topological charge +½ could merge together at a sufficiently small separation, forming a +1 defect and causing the cells within to "escape into the third dimension" by standing up vertically. We hypothesized that this process could only occur if the merging comets generated sufficient force to overcome

the repulsion between them, potentially explaining why only the higher activity $\Delta pilH$ cells become trapped in place. To test this possibility, we first extended our SPR model to three dimensions to allow rods to reorient out of the plane and simulated collisions between comets (Methods). Stable structures of upright rods ("rosettes") formed once the rods' propulsive force, F, increased beyond a critical threshold, F_v, confirming our intuition (Fig. 4a, Extended Data Fig. 5, Supplementary Videos 7, 8). $\Delta pilH$ cells are also slightly longer than WT cells (Extended Data Fig. 6a), but this acts to suppress the nucleation of rosettes rather than promote it[22] (Extended Data Fig. 6b-e, Supplementary Notes). To test if the increased force generated by $\Delta pilH$ cells is alone sufficient to preferentially trap them in rosettes, we next used our 3D SPR model to simulate the interaction of two different genotypes that each exert a different propulsive force (Fig. 4b, c). This showed that higher-force mutants, on average, move more slowly than the WT cells because a larger fraction of the higher-force mutants become stuck in rosettes where their movement is arrested.

We tested these theoretical predictions by inoculating subsurface colonies composed of a mixture of both $\Delta pilH$ and WT cells. In these colonies, we observed that $\Delta pilH$ cells spontaneously formed rosettes, whereas WT cells did not (Supplementary Video 5). Moreover, we were able to quantify the movement of topological defects when the fraction of $\Delta pilH$ cells in the front begins to sharply decrease (Fig. 2f). We observed comets approaching each other (Fig. 4d) before the monolayer of cells began to reorient out of plane, forming a rosette with a stable topological charge of +1 (Fig. 4e, Extended Data Fig. 7, Supplementary Video 9) as predicted by our SPR model (Fig. 4a). Even though this colony was initiated with an equal fraction of WT and $\Delta pilH$ cells, confocal imaging revealed that the core of this rosette was nearly entirely composed of vertically oriented $\Delta pilH$ cells (Fig. 4f). Once initiated, rosettes in both experiments and simulations grew larger in size (Supplementary Videos 8, 9). These dynamics are reminiscent of the "inverse domino" cascade of cell verticalization seen at the

centre of non-motile *Vibrio cholerae* bacterial colonies when they reach a critical size[22,23], which is instead driven by buckling induced by cell division[22].

The direct observation of rosettes in our experiments and their close correspondence with those observed in our models provides strong evidence that Δ*pilH* cells become trapped as a direct consequence of their higher activity. However, we also considered other possible pleiotropic effects of this mutation, such as an increase in doubling times[24] and cell-cell adhesion[24,25]. Extensive analyses rule these out as explanations of the sudden decline of the fraction of Δ*pilH* cells at the colony front (Supplementary Notes, Extended Data Figs. 8, 9). We also considered whether a deficiency in chemotaxis might play a role in the slower expansion of Δ*pilH* cells. We could not directly confirm, however, if chemotaxis plays any role in colony expansion in our assays because the only known mutant deficient in pili-based chemotaxis, Δ*pilG*[18], shows little, if any, motility under agar (likely because they produce relatively few pili[17,18], Supplementary Notes, Extended Data Fig. 1c). We decided that a more straightforward and definitive test of whether rosette formation was responsible for Δ*pilH* cells' reduced capacity to spread was to cover colonies with progressively stiffer agar, which acts to increase the stabilising torque that resists cell verticalization (Methods, Eq. 7). Increasing the agar concentration of the overlying pad was observed to both dramatically suppress the formation of rosettes and allow Δ*pilH* cells to expand much further before they were fully displaced by WT cells (*e.g.* stiffer agar increased the proportion of Δ*pilH* cells in the front by 80-fold after 1.2 mm of collective expansion, Supplementary Notes, Extended Data Fig. 10). These experiments, along with the observations that the proportion of Δ*pilH* cells in the front only begins to decrease once cells transition from individual to collective motility and start to form rosettes (Fig. 2e,f, Supplementary Videos 5, 9), strongly suggest that the loss of Δ*pilH* cells from the front of mixed colonies is caused primarily by their tendency to become trapped in rosettes, rather than due to a deficiency in chemotaxis or another putative mechanism.

6

Recently, two preliminary reports have shown wild-type *P. aeruginosa* and *Myxococcus xanthus* cells can form multiple layers of horizontally aligned cells when moving collectively using pili-based motility[26,27]. While we also observe that both WT and Δ*pilH* cells form these terrace-like structures at the very edge of our colonies (Extended Data Fig. 10c), their morphology and distribution is very different to the verticalized rosettes, which occur deeper within the colony and are dominated by the faster moving Δ*pilH* cells . Nevertheless, these new studies contribute to our understanding of the diverse physical mechanisms that dictate the architecture of bacterial colonies and further illustrate how they can serve as model systems of active matter[20,22,23,26–29].

Our results show that the physics of active liquid crystals can exert a fundamental limit on the speed of motility within crowds of bacteria. Cells that exceed this critical threshold form high-velocity comets that are unstable to verticalization upon collision, causing fast-moving cells to become trapped within the interior of colonies where nutrients are scarce[30]. However, bacteria that move more slowly as individuals are able to avoid this fate and collectively expand faster. In the race into new territory, the physical processes we describe therefore favour bacteria that exercise restraint by moving slowly and prudently.

1. Nadell, C. D., Drescher, K. & Foster, K. R. Spatial structure, cooperation and competition in biofilms. *Nat. Rev. Microbiol.* **14**, 589–600 (2016).

2. Zhang, H. P., Be'er, A., Florin, E.-L. & Swinney, H. L. Collective motion and density fluctuations in bacterial colonies. *PNAS* **107**, 13626–30 (2010).

3. Gloag, E. S. *et al.* Self-organization of bacterial biofilms is facilitated by extracellular DNA. *PNAS* **110**, 11541–6 (2013).

4. Wu, Y., Kaiser, A. D., Jiang, Y. & Alber, M. S. Periodic reversal of direction allows Myxobacteria to swarm. *PNAS* **106**, 1222–7 (2009).

5. Shrivastava, A. *et al.* Cargo transport shapes the spatial organization of a microbial community. *PNAS* **115**, 8633–8638 (2018).

6. Talà, L., Fineberg, A., Kukura, P. & Persat, A. Pseudomonas aeruginosa orchestrates twitching motility by sequential control of type IV pili movements. *Nat. Microbiol.* **4**, 774–780 (2019).

7. Skerker, J. M. & Berg, H. C. Direct observation of extension and retraction of type IV pili. *PNAS* **98**, 6901–4 (2001).

8. Doostmohammadi, A., Ignés-Mullol, J., Yeomans, J. M. & Sagués, F. Active nematics. *Nat. Commun.* **9**, 3246 (2018).

9. Mermin, N. D. The topological theory of defects in ordered media. *Rev. Mod. Phys.* **51**, 591–648 (1979).

10. Giomi, L., Bowick, M. J., Mishra, P., Sknepnek, R. & Cristina Marchetti, M. Defect dynamics in active nematics. *Philos. Trans. A.* **372**, 20130365 (2014).

11. Giomi, L., Bowick, M. J., Ma, X. & Marchetti, M. C. Defect Annihilation and Proliferation in Active Nematics. *PRL* **110**, 209901 (2013).

12. Gennes, P. G. de. & Prost, J. *The physics of liquid crystals.* (Clarendon Press, 1993).

13. Meyer, R. B. On the existence of even indexed disclinations in nematic liquid crystals. *Philos. Mag.* **27**, 405–424 (1973).

14. Jarrell, K. F. & McBride, M. J. The surprisingly diverse ways that prokaryotes move. *Nat. Rev. Microbiol.* **6**, 466–476 (2008).

15. Wensink, H. H. *et al.* Meso-scale turbulence in living fluids. *PNAS* **109**, 14308–13 (2012).

16. Dunkel, J. *et al.* Fluid Dynamics of Bacterial Turbulence. *PRL* **110**, 228102 (2013).

17. Bertrand, J. J., West, J. T. & Engel, J. N. Genetic Analysis of the Regulation of Type IV Pilus Function by the Chp Chemosensory System of Pseudomonas aeruginosa. *J. Bacteriol.* **192**, 994–1010 (2009).

18. Oliveira, N. M., Foster, K. R. & Durham, W. M. Single-cell twitching chemotaxis in developing biofilms. *PNAS* **113**, 6532–6537 (2016).

19. Kim, W., Racimo, F., Schluter, J., Levy, S. B. & Foster, K. R. Importance of positioning for microbial evolution. *PNAS* **111**, E1639-47 (2014).

20. Dell'Arciprete, D. *et al.* A growing bacterial colony in two dimensions as an active nematic. *Nat. Commun.* **9**, 4190 (2018).

21. Doostmohammadi, A., Thampi, S. P. & Yeomans, J. M. Defect-Mediated Morphologies in Growing Cell Colonies. *PRL* **117**, 048102 (2016).

22. Beroz, F. *et al.* Verticalization of bacterial biofilms. *Nat. Phys.* **14**, 954–960 (2018).

23. Drescher, K. *et al.* Architectural transitions in Vibrio cholerae biofilms at single-cell resolution. *PNAS* **113**, E2066-72 (2016).

24. Oldewurtel, E. R., Kouzel, N., Dewenter, L., Henseler, K. & Maier, B. Differential interaction forces govern bacterial sorting in early biofilms. *Elife* **4**, e10811 (2015).

25. Anyan, M. E. *et al.* Type IV pili interactions promote intercellular association and moderate swarming of Pseudomonas aeruginosa. *PNAS* **111**, 18013–8 (2014).

26. Takatori, S. C. & Mandadapu, K. K. Motility-induced buckling and glassy dynamics regulate three-dimensional transitions of bacterial monolayers. Preprint at https://arxiv.org/abs/2003.05618. (2020).

27. Copenhagen, K., Alert, R., Wingreen, N. S. & Shaevitz, J. W. Topological defects induce layer formation in Myxococcus xanthus colonies. Preprint at https://arxiv.org/abs/2001.03804. (2020).

28. Grant, M. A. A., Wacław, B., Allen, R. J. & Cicuta, P. The role of mechanical forces in the planar-to-bulk transition in growing Escherichia coli microcolonies. J. R. Soc. Interface **11**, 20140400 (2014).

29. Yaman, Y. I., Demir, E., Vetter, R. & Kocabas, A. Emergence of active nematics in chaining bacterial biofilms. Nat. Commun. **10**, 2285 (2019).

30. Pirt, S. J. A Kinetic Study of the Mode of Growth of Surface Colonies of Bacteria and Fungi. Microbiology **47**, 181–197 (1967).
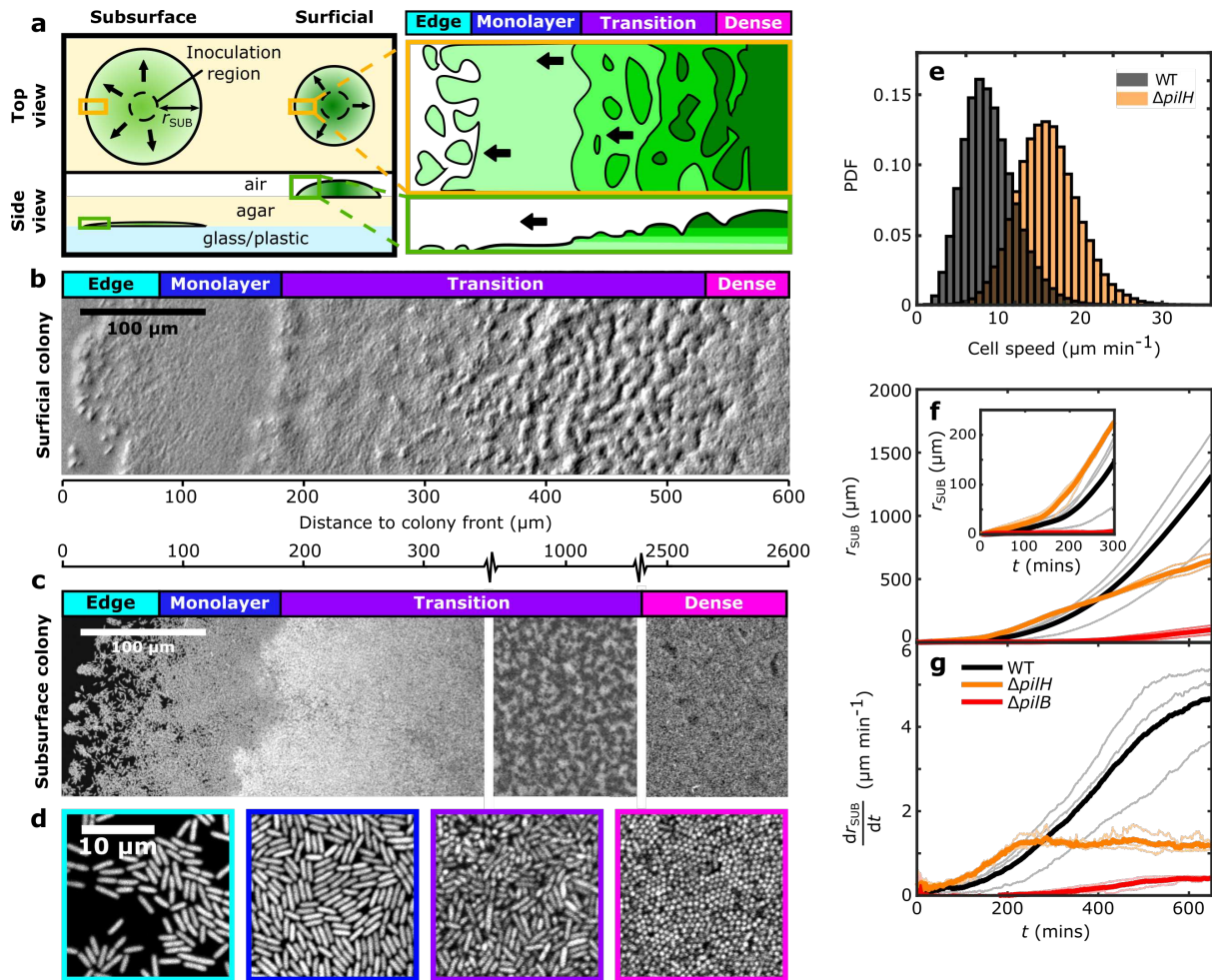
Fig. 1 | Pili-based motility drives the spread of *P. aeruginosa* colonies, but cells that individually move faster spread more slowly. **a**, Both subsurface colonies, which grow beneath a layer of agar, and surficial colonies, which grow on top of agar, consist of four distinct regions. **b**, **c**, **d**, The "edge" contains small groups of loosely packed cells, the "monolayer" is composed of tightly packed cells lying flat against surface, the "transitional" region is a mixture of horizontally and vertically oriented cells, and in the "dense" region almost all cells are vertical. Panel **d** shows magnified views of each subsurface colony region. **e**, The probability density function (PDF) of the speed of individual WT and Δ*pilH* cells within the monolayer region. **f**, **g**, Measurements of the subsurface colony radius, r_{SUB}, and expansion rate, dr_{SUB}/dt for monocultures of WT (black), Δ*pilH* (orange) and non-piliated Δ*pilB* (red) cells. Inset in **f** shows a magnified view of the first 300 mins. Bold lines in **f**, **g** indicate the mean of three separate experiments.
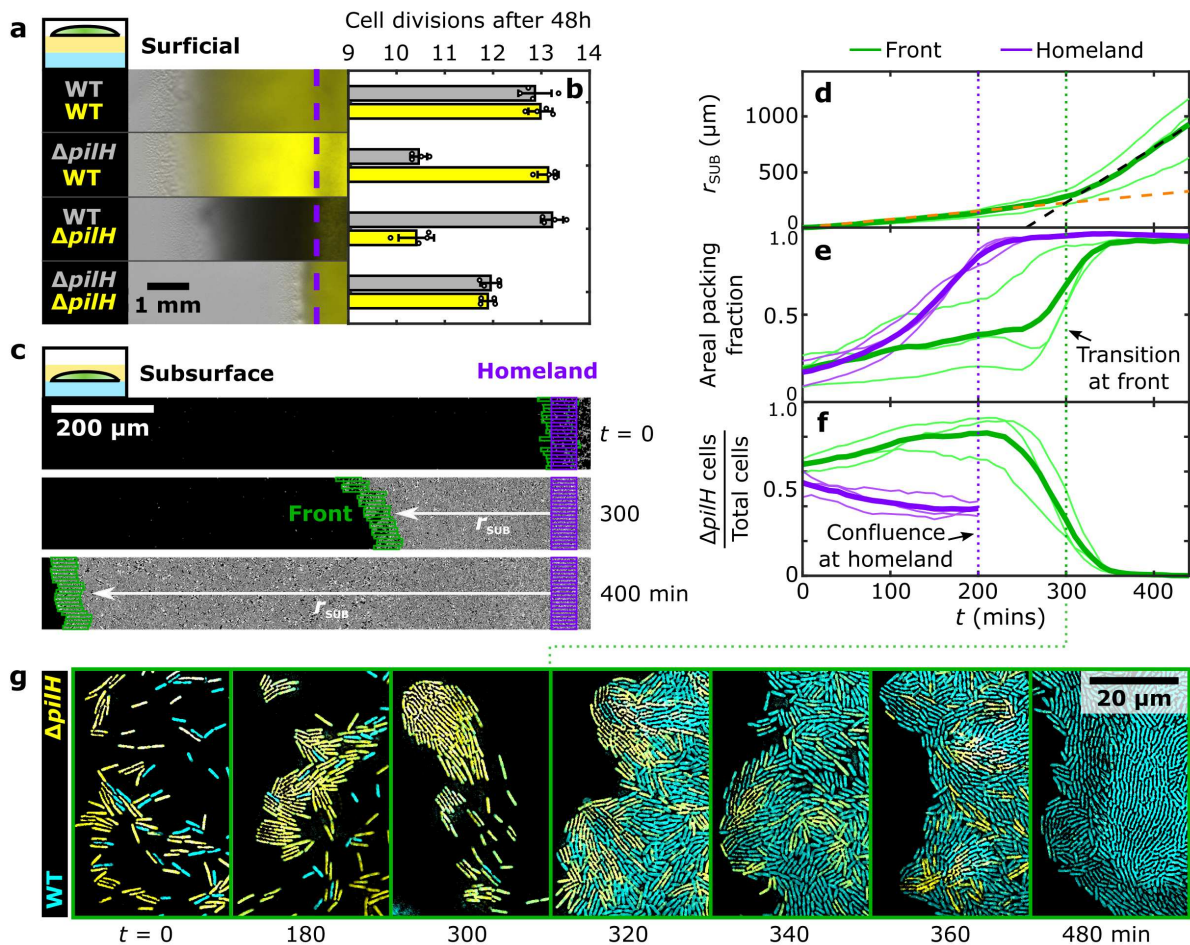
Fig. 2 | WT cells outcompete Δ*pilH* cells when mixed together in the same colony. a, Surficial colonies inoculated with equal proportions of YFP and CFP labelled cells after 48 hours. Dashed purple lines indicate the boundary of the "homeland", the region where cells are initially inoculated onto the agar. Due to imaging constraints (Methods), we show only the YFP and brightfield channels. Both strains appear in the latter, so regions with more CFP-labelled cells appear darker. **b**, Number of cell divisions occurring over 48 hours of incubation within colonies shown in **a**. Grey and yellow bars denote populations labelled with CFP and YFP, respectively. Error bars show the standard deviation of 4 replicates. **c**, Subsurface colonies were initialized with equal proportions of YFP labelled Δ*pilH* and CFP labelled WT cells. We analysed dynamics within both the homeland (stationary, purple boxes) and the "front" of the colony, which follows the edge of the colony has it expands (green boxes, Supplementary Video 4). **d**, Measurement of the distance between the front and homeland regions, r_{SUB}, reveals a seven-fold increase in colony expansion rate at $t = 300$ mins (dashed lines, fitted with piecewise linear regression). The areal packing fraction (the fraction of the surface covered by cells) (**e**), and the relative frequency of Δ*pilH* cells (**f**) at the front also show sharp transitions at $t = 300$ mins. Bold lines in **d-f** indicate the mean from three separate experiments. Upon reaching confluence at $t = 200$ mins, cells in the homeland became too tightly packed to resolve their identity. **g**, Magnified images of the leading edge of a subsurface colony initiated with equal fractions of WT (cyan) and Δ*pilH* (yellow) cells. These images were processed as described in the Methods.
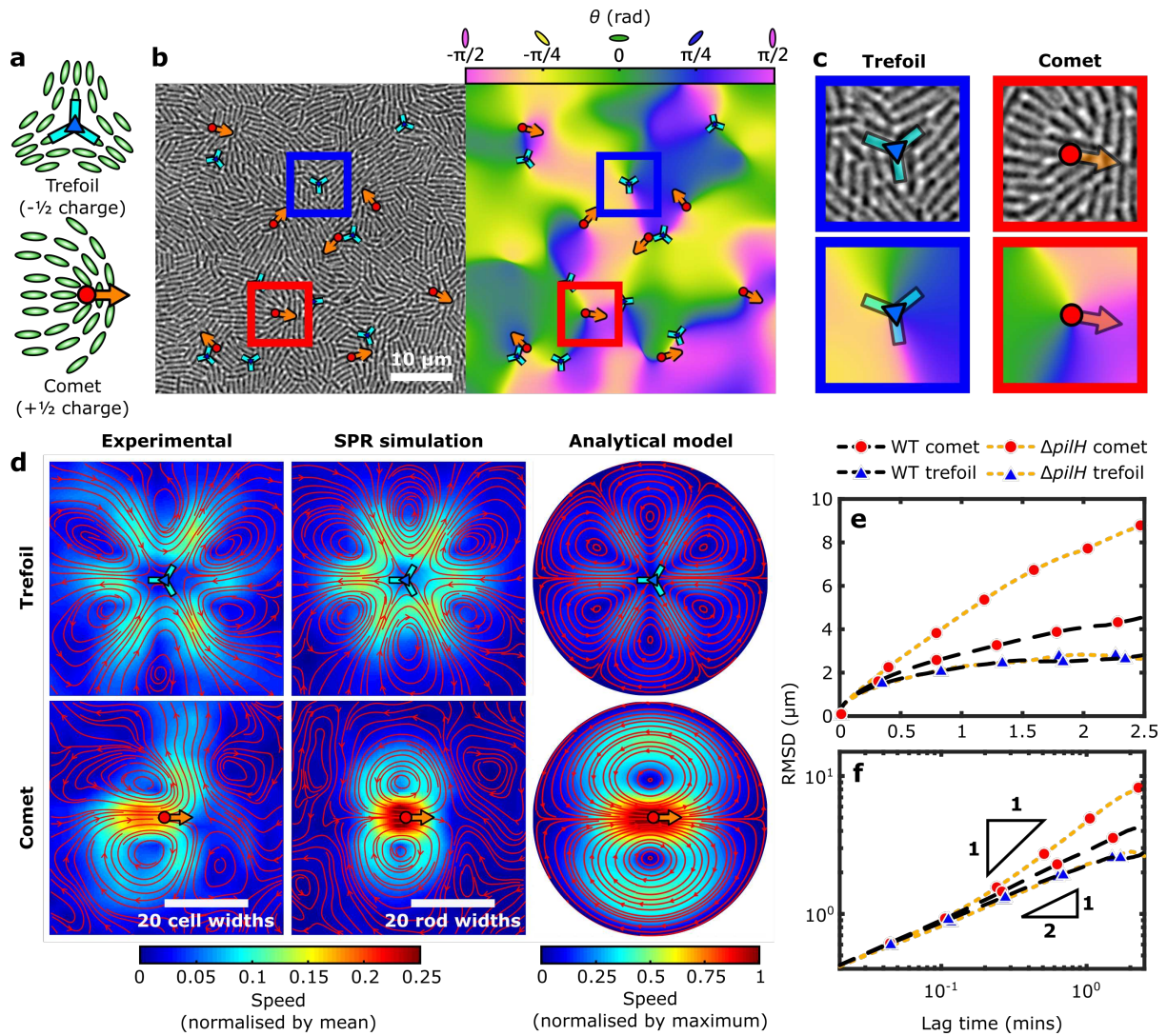
11

Fig. 3 | Subsurface colonies exhibit patterns of collective motility consistent with a nematic system driven out of equilibrium. a, Two types of topological defects occur in 2D nematic systems: trefoils, which exhibit three-fold rotational symmetry and have a topological charge of -1/2, and comets, which migrate along their single axis of symmetry and have a charge of +1/2 (see text). **b**, The locations and orientations of defects in the monolayer of a WT subsurface colony (left, Supplementary Video 6) were obtained by quantifying the local cell orientation (right). **c**, Magnified views of the red and blue boxes in **b** illustrate how defects occur at singularities in cell orientation. **d**, Simultaneous tracking of both defects and individual cells within a monolayer (Supplementary Videos 2, 6) allows the mean cell flow around defects to be resolved. The structure of the flow closely resembles that predicted from a self-propelled rod (SPR) simulation and an analytical model (Methods). Red lines show streamlines and the background colours indicate flow speed. **e**, **f**, The root mean squared displacement (RMSD) measures how far defects move over a given lag time, plotted here on both a linear (**e**) and logarithmic scale (**f**). Triangles in **f** show the slopes predicted for ballistic (1:1) and diffusive (1:2) movement.
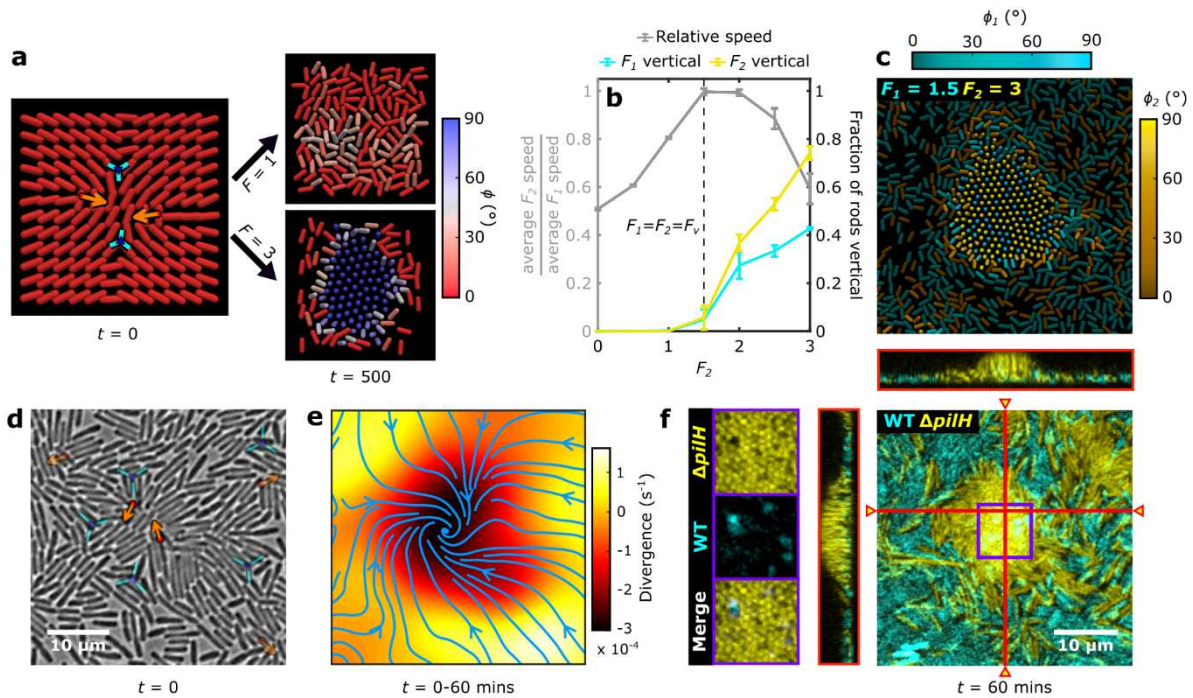
12

Fig. 4 | Δ*pilH* cells are preferentially trapped by rosettes, preventing their outward migration. a, A 3D SPR simulation of two comets colliding with one another shows that rods propelled by smaller force (*F*=1) remain flat against the surface after an initial transient, while those propelled by a larger force (*F*=3) form a stable, vertically oriented rosette (Supplementary Video 7). Colour denotes the angle of rods relative to the surface, ϕ. **b**, SPR simulations initialized with randomly oriented rods, half of which are propelled by a fixed force of $F_1=F_v$=1.5 (cyan, "WT") and the other half by a variable force F_2 (yellow, "mutant"). The left axis shows the mean speed of the F_2 population at steady-state normalized by that of the F_1 population. The right axis indicates the fraction of each population that is vertically oriented (defined as $\phi > 85°$). Error bars indicate standard deviation of three different simulations, each with a different random initial configuration. **c**, A rosette from a F_1=1.5, $F_2 = 3$ simulation at steady-state, where ϕ_1 and ϕ_2 denote the orientation of the two respective populations. **d**, Two comets approaching one another in a colony initiated with an equal number of WT and Δ*pilH* cells (Supplementary Video 9). **e**, Measurements of cell velocity within same region as **d** during rosette development. Blue arrows and colormap respectively show streamlines and divergence of the time-averaged flow field (Methods). Regions of negative divergence indicate zones of cell accumulation. **f**, Three-dimensional confocal image of the rosette that formed within the same region shown in **d** and **e**, taken 60 mins after **d** (Methods). Vertical slices through the rosette are shown to the top and right, at locations indicated by triangles. (**f, inset**) A magnified view of the rosette (purple box in **f**) shows is it mostly composed of Δ*pilH* cells in a vertical orientation. Main panel shows maximal *z*-projection of both YFP and CFP channels, while insets show individual *z* slices.